Covalent organic framework incorporated outer-selective hollow fiber thin-film nanocomposite membranes for osmotically driven desalination

Sungil Lim[1], Nawshad Akther[1], Van Huy Tran[1], Tae-Hyun Bae[2], Sherub Phuntsho[1], Andrea Merenda[3], Ludovic F. Dumée[3], and Ho Kyong Shon[1]*

[1]*Centre for Technology in Water and Wastewater, School of Civil and Environmental Engineering, University of Technology Sydney (UTS), Australia*

[2]*Department of Chemical and Biomolecular Engineering, Korea Advanced Institute of Science and Technology, Republic of Korea*

[3]*Geelong Institute for Frontier Materials, Deakin University, Australia*

* Corresponding author: Prof. Ho Kyong Shon Email: hokyong.shon-1@uts.edu.au; Tel.: +61 2 9514 2629; Fax: +61 2 9514 2633.

Abstract

In this study, new outer-selective hollow fiber (OSHF) thin film nanocomposite (TFN) forward osmosis (FO) membranes incorporated with amine-rich Schiff-based network (SNW-1) nanoparticles (NPs), a type of covalent organic frameworks (COFs), were developed by vacuum-assisted interfacial polymerization (VAIP). The SNW-1 NPs possess hydrophilic nature and porous internal structures, which are desirable for producing highly permeable and efficient FO membranes. SNW-1 NPs were conformally packed across the outer surface of the HF substrate by vacuum pressure applied during the VAIP process leading to defect-free coatings. Furthermore, covalent bonding between secondary amine (NH_2^-) groups across the SNW-1 network and remanent carboxylic groups present from the monomer used for the interfacial polymerization step supported the adhesion of SNW-1 NPs to the native poly(amide) layer present across the TFN membrane surface. As a result, SNW-1 loading at 0.001 wt. % exhibited the best FO performance with enhanced water flux more than 23% of the pristine one (31.5 L m^{-2} h^{-1}) and relatively low specific reverse solute flux (SRSF, J_s/J_w) at 0.18 g L^{-1} using 1 M NaCl and DI water in series of TFN composite membranes. The optimum loading at 0.001 wt% was much lower than those in other home-made TFN membranes (normally above 0.05 wt. %) due to the minimum loss of SNW-1 in the VAIP. Also, the TFN membrane offered excellent FO operation stability tested for 72 h. Such novel approach is promising to optimize FO processes for desalination and water treatment in the future.

Keywords: Covalent organic frameworks; Forward osmosis; Outer-selective hollow fiber; Schiff-based network; Thin-film nanocomposite

1 Introduction

FO membrane processes have been recently vitalized for low-energy desalination [1-4], wastewater treatment [5-7], food processing [8] and energy harvesting [9, 10]. Unlike pressure-driven membrane processes for water treatment such as microfiltration (MF), ultrafiltration (UF), nanofiltration (NF) and reverse osmosis (RO) filtration, the driving force of FO processes is naturally produced by the osmotic pressure between high saline water and low saline feed water contained with impurities across a semi-permeable membrane. Since there is no requirement for applied hydraulic pressure under FO operation, advantages of the FO processes for water treatment and desalination include lower energy consumption and less fouling potential than conventional RO processes. In addition, various FO hybrid applications have been investigated such as FO-RO hybrid process for low-energy desalination, osmotic membrane bioreactor (OMBR) with aerobic or anaerobic digestions for wastewater treatment, fertilizer-drawn FO (FDFO) processes for fertilizer irrigation in agricultural area [2, 11-13].

Although FO represents an emerging eco-friendly membrane technology for desalination or other water treatment processes, there are existing obstacles to optimize and demonstrate large-scale FO applications. One major challenge is related to identifying the suitable draw solution for energy- and cost-effective regeneration [14-17]. The second challenge is related to the design of the membrane materials requiring to be further tune to match FO requirements. FO membranes should be highly permeable to water, strictly ion selective, mechanically stable and provide anti-fouling performance to enhance the membrane durability and cost-effectiveness of the process [18-20]. Based on these requirements, recently developed and commercial FO membranes were mainly developed as thin-film composite (TFC) membranes, which consist of a thin polyamide (PA) active layer, a porous membrane substrate and backing fabric. The main advantage of TFC membranes is that each layer may be individually customized to improve membrane performance. Performance during FO process relies on both

the mitigation of internal concentration polarization (ICP) and the control of water transport across the surface and free volume of the TFC membranes respectively [21-23]. Although the selective outer layer plays an important role over the operation, the development of highly permeable and ion selective TFC FO membranes with higher water and solute permeabilities is challenging the trade-off between water flux and reverse solute diffusion [23-26].

New strategies to alter the intrinsic transport properties of FO membranes for enhancing membrane performance were investigated [27-29]. Several studies demonstrated the modification of membrane substrate or PA active layer by incorporating various hydrophilic nanomaterials such as graphene oxide and silica [30-33]. Representative hydrophilic nanofillers including carbon-based nanomaterials such as functionalized graphene, graphene oxide [34-37], functionalized carbon nanotubes [38, 39] and carbon quantum dots [40, 41], inorganic nanomaterials such as silica, zeolite and halloysite nanotubes [42, 43], and metal-based nanoparticles (NPs) like Ag and TiO_2 [29] have been considered as nanofillers to incorporate into a membrane substrate for mixed matrix membranes or into a PA selective layer for thin-film nanocomposite (TFN) FO membranes [24].

In addition, various kinds of framework-based materials such as metal-organic frameworks (MOFs), covalent-organic frameworks (COFs) and zeolitic imidazolate frameworks (ZIFs) has been investigated as a new category of nanofillers for developing nanocomposite membranes [23, 31, 44, 45]. COFs especially possess highly microporous structures, tuneable chemical functionalities and an ability for selective grafting with various chemistries due to the organic linkers on the building blocks [23, 31, 44]. These unique characteristics of COFs may contribute to customize the physicochemical properties of polymeric membranes to be highly water permeable due to their porous structures and hydrophilicity. Our previous study presented that the flat-sheet TFN membranes incorporated with amine-rich Schiff-based network-1 (SNW-1) COFs into PA layer were recently developed

for FO applications [46]. That study mentioned that the porous SNW-1 NPs inside PA layer produced more pathways for water transport from its porous morphology, higher hydrophilicity from high density of amine-based functional groups and better compatibility with a thin PA layer due to covalent bonding with the acyl chloride in interfacial polymerization (IP) processes. As a novel nanofiller, COFs including SNW-1 may be used to fabricate a highly permeable polymeric membrane, when the COFs are located inside a thin PA layer by their own characteristics.

In our previous studies, successful development of outer-selective hollow fiber (OSHF) TFC membranes for FO applications was reported, exhibiting specific advantages for FO applications [47-49]. Furthermore, COF SNW-1 porous NPs were effectively used to produce high-permeable TFN FO membranes from literature [46]. To the best of our knowledge, we for the first time aim to successfully develop outstanding OSHF TFN membranes using the SNW-1 NPs for enhancing water permeability with stable integrity of the PA/SNW-1 composite layer. A new hypothesis of conceptual methodologies and expected formation mechanisms incorporating SNW-1 into the PA active layer of OSHF TFN membranes was proposed. Then, the OSHF TFN membranes were subsequently designed and fabricated, following the proposed hypothesis. We finally evaluated the performance of nascent OSHF TFN membranes using lab-scale tests on key FO performance parameters and membrane stability over long-term experiments.

2 Materials and methods

2.1 Materials and chemicals

For preparing HF membrane substrates, poly(ethersulfone) powder (PES, Veradel® 3000P, Solvay) with the molecular weight at 63,000 g/mol and 1-methyl-2-pyrrolidone (NMP, Merck) as a solvent of PES were used. As an additive for altering pore formation, poly(ethylene glycol) 400 (PEG400, Sigma-Aldrich) at 5 wt. % was mixed into the polymer solution. For conducting interfacial polymerization to form a PA layer on the membrane substrate, amine-based 1, 2-phenylenediamine (MPD, 99%, Sigma-Aldrich) aqueous solution and chlorine-based trimesoyl chloride (TMC, 98%, Sigma-Aldrich) in organic solution was used. For long-term storage of HF membranes, membrane substrates were immersed into the glycerol-based aqueous solution (50/50 wt. %) for 24 h and subsequently dried in air in order to reserve surface and internal morphology of HF membrane substrates. As a nanofiller for TFN membranes, home-made COF as denoted as SNW-1 was synthesized with Melamine (99%, Macllin Reagent), terephthalaldehyde (98%, Macllin Reagent) and dimethyl sulfoxide (DMSO, analytical grade, Sinopharm Chemical Reagent) as key materials for its synthesis and dichloromethane, tetrahydrofuran (THF) and acetone manufactured by Sinopharm Chemical Reagent for the post-treatment of SNW-1. For FO performance tests, Deionized water with the resistivity at 18 MΩ/cm (Milli-Q, Millipore) and sodium chloride (Chem Supply) were employed as FS and draw solution, respectively.

2.2 Preparation of hollow fiber membrane substrates

The spinning parameters to fabricate the HF membrane substrates for preparing OSHF TFC membranes were optimized in our previous study [48]. The dry-jet wet spinneret machine was used to cast HF membrane substrates. Dried PES powder was dissolved in NMP solution

at 16.5 wt. % with an additive of PEG400 at 5 wt. % for 12 h using the temperature-controlled magnetic stirrer (AREC, VELP Scientifica). The prepared dope solution was pre-filtered by fabric mesh to remove undesirable impurities and bubbles. After that, the prepared dope solution was placed in the syringe pump (Model 500D, Teledyne ISCO) and left overnight to degas. In the membrane casting, the specific spinning parameters were confirmed and tabulated in Table S1 as what we optimized to prepare HF membrane substrates for subsequent polyamide (PA) active layer deposition via the VAIP method in our previous study [48]. Prepared HF membrane substrates were stored in DI water for 2 days to remove solvents occupied in polymeric layers fully, and then immersed in glycerin-based aqueous solution for 12 h and dried in the atmosphere for their long-term preservation.

As aforementioned, for installing laboratory-scale membrane modules, two fibers of membrane substrates in the length of 13.5 cm were prepared and carefully spaced inside customized acryl module for subsequent FO performance tests. Each edge of membrane fibers in the modules were capped by potting with a general epoxy resin with retaining their bore holes at each side. The effective surface area was estimated at 6.5 cm^2 per each module.

2.3 Preparation of OSHF TFN membranes using SNW-1

As the main nanofiller, the COF NPs denoted as SNW-1 was synthesized by using the solvothermal method as described elsewhere [46, 50]. For preparing OSHF TFN membranes, our modified vacuum-assisted interfacial polymerization (VAIP) was applied with amine-based MPD aqueous solution and chlorine-based TMC organic solution. The detailed methodological procedure of the modified VAIP for OSHF TFC membranes was described in detail in our paper [51]. To prepare these solutions, the SNW-1 powder was suspended in DI water and sonicated by the laboratory-scale sonicator for over 6 h. The loading of SNW-1 in

158 DI water was varied in the range of 0 to 20 mg L^{-1}, and then the MPD flake at 2 wt. % and SDS
159 powder at 0.2 wt. % were added and mixed into the SNW-1 spiked DI water by a magnetic
160 stirrer under room atmosphere. After the VAIP process, the prepared OSHF TFN membrane
161 was washed by DI water several times and subsequently stored in DI water at 4 °C for its future
162 testing. In this study, the SNW-1 loading was varied from 0 to 0.002 wt.%, and the prepared
163 OSHF TFN membranes were denoted as S# according to SNW-1 loading as shown in Table 1.

164

165 **Table 1** Chemical compositions of the VAIP process for OSHF membrane samples.

TFN membranes	Chemical composition in solvent		
	MPD/SDS in water (wt. %)	TMC in n-Hexane (wt. %)	SNW-1 loading (wt. %)
S0	2 / 0.2	0.15	0
S3			0.0003
S5			0.0005
S10			0.0010
S15			0.0015

166

167 **2.4 Characterization of OSHF TFN membranes with SNW-1**

168 For observing surface and internal morphologies of membrane samples, the field
169 emission scanning electron microscope (FESEM, Carl Zeiss AG) was mainly used with an
170 accelerating voltage of 5–10 kV. Before conducting the SEM analysis, the specimens were
171 placed on the aluminium stubs, and then they were fully dried by N_2 compressed gas.
172 Subsequently, the samples were coated with a 10-nm gold-palladium (Au-Pd) layer with a
173 metal sputtering machine (EM ACE600, Leica). In addition, for characterizing chemical
174 changes of membrane samples, a fourier transform infrared spectroscopy (FTIR, Affinity-1,

175 Shimadzu) was used under the signal range of 800 to 2000 cm^{-1} (Signal resolution at 1 cm^{-1}
176 and minimum 16 scans). The surface topography was analyzed by the atomic force microscopy
177 (AFM, Park XE-7, Park Systems) under the atmosphere tapping and scanning at 5 to 5 μm, and
178 the image software was used to determine the mean roughness of the samples. Moreover, the
179 membrane's hydrophilicity was confirmed by using the sessile-drop optical subsystem (Theta
180 Lite 100, Biolin Scientific) including its image-analysis program.

181

182 **2.5 FO performance of OSHF TFN membranes**

183 The FO performance test was conducted to evaluate intrinsic FO performance of home-
184 made OSHF TFN membranes using the lab-scale FO unit described elsewhere [36, 48]. For
185 the test, HF membrane modules including a series of TFN FO membranes were prepared and
186 assembled into the FO test unit. The membrane orientation under the testing operation was AL-
187 FS (FO mode) which means that FS is facing to the active layer in the module. The driving
188 force of the FO operation was produced by the osmotic pressure between 1 M NaCl solution
189 as DS and deionized water as FS. The cross-flow velocity of feed and draw stream was 20.9
190 cm/sec and 10.4 cm/sec under co-current flow mode, respectively. Temperatures of both FS
191 and DS were stably controlled at 23 ± 0.5°C by using the temperature controller.

192 For the evaluation of FO performances, water flux (J_w), reverse salt flux (J_s) and
193 specific reverse solute flux (SRSF, J_s/J_w) of FO membranes were indirectly determined by the
194 change in mass and concentration of the FS, respectively. The detailed methods are described
195 in SI. Furthermore, the water flux and SRSF of OSHF membrane samples were determined as
196 a function of the concentration of draw solution from 0.5 to 2 M NaCl (0.5, 1, 1.5 and 2 M)
197 under the FO operation above in order to investigate the trend of FO performance according to
198 different osmotic pressure. With the trend of FO results, the water permeability (A), solute

permeability coefficient (*B*) and intrinsic selectivity (*B/A*) of hollow fiber TFC membranes were estimated by using the 4-stages model algorism developed by Tiraferri et al. [52] for determining intrinsic transport property of the membrane samples. Some literature in FO research applied this model estimation to determine *A*, *B* and *S* values and the estimated values were subsequently compared to evaluate membrane's intrinsic transport properties. Detailed information about the model calculation is described elsewhere [36, 52].

The long-term operating test for 3 days was conducted to offer a more reliable and practical evaluation of the membrane's performance and stability. In this test, the best membrane candidate in the FO performance test was selected to conduct the stability test. The selected FO membrane was operated under the typical FO operation over 72 h, and the feed and draw solution were refreshed every 12 h in order to minimize the osmotic dilution in the FO process. The water flux and RSF of the membrane samples in the stability test were continuously monitored.

3 Results and discussion

3.1 Characterizations of SNW-1 NPs for fabricating OSHF TFN membranes

As the key nanofiller, the COF based SNW-1 NPs were used for preparing the OSHF TFN membranes in this study. The produced SNW-1 NPs were observed as a uniform and smooth spherical shape in the size range of 20-40 nm as presented in Fig. 1. The Brunauer-Emmet-Teller (BET) surface area, Non-Localized Density Functional Theory (NL-DFT) volume and mean pore size of the SNW-1 NPs were 500 m^2 g^{-1} and 0.14 cm^3 g^{-1} and 5.5 Å, respectively [46]. Another study also presented similar physical properties of their home-made SNW-1 NPs with our one [44]. The SNW-1 NPs are made of melamine-based porous organic-based frameworks, and Gao et al. and Akther et al. reported that the average internal pore size of SNW-1 NPs was calculated at around 5 Å [46, 53]. As shown in Fig. S1(a), for TFN membranes with SNW-1, the porous internal structures of SNW-1 may provide sub-1 nm extra water channels inside a dense PA layer [44, 46, 53]. In addition, small and smooth external shape of SNW-1 NPs (Fig. S1(b)) may contribute to embedding the NPs into a thin PA layer with less deterioration of the layer's integrity. The SNW-1 NPs were well dispersed in DI water due to the existence of the secondary amine group on the SNW-1's surface. This is because SNW-1 NPs possess strong affinity for water molecules presented in Fig. S1(c), which can be a preferable property for developing TFN membranes [46].

In typical IP processes for preparing TFN membranes, hydrophilic nanofillers are normally blended with the MPD solution, and the mixed MPD solution is initially immersed on a membrane substrate. After allowing for specific time for absorbing the solution into surface pores, excess MPD solution on the surface is generally removed by nitrogen flushing or rubber roller. At that time, it is expected that excess nanofillers across the membrane surface may be removed so that the effective nanofillers loading may be accurately performed. The

expected phenomenon is illustrated in Fig. 1. Unlike the general IP process, the excess MPD solution on the surface of a HF substrate is removed by suction to inside the HF substrate at the specific vacuum pressure in the VAIP process. At the same time, loosely settled SNW-1 NPs across the surface can be strongly accumulated by the vacuum pressure onto the bottom as illustrated in Fig. 1 (a) so that most SNW-1 NPs could be placed on the surface with less particle loss. Subsequently, the stacked SNW-1 NPs on the surface and MPD solution inside the pores would be reacted with the organic TMC solution, and at the same time the deposited SNW-1 NPs would be properly embedded into the PA layer. For supporting the hypothesis, we found that optimum concentrations of nanofillers in other related studies were mainly over 0.05 wt. % under the general IP, which is over 50 times more than the optimum SNW-1 loading (0.001 wt. %) under the VAIP in this study [33]. Thus, employing VAIP technique can contribute towards reducing the production cost of TFN FO membranes by minimizing nanoparticle loss during the fabrication process. Furthermore, as presented in Fig. 1 (c), the secondary amine groups surrounding the SNW-1 may react with the acyl chloride groups in TMC solution under the IP process, and the strong covalent bonds would be subsequently formed between SNW-1 and TMC solution [44]. The formed amide-based thin layer on the SNW-1 may positively affect the integrity of the PA composite layer with minimizing the voids or defects from SNW-1. It thus hypothesizes that the SNW-1 NPs might be properly incorporated into a thin PA layer in the VAIP based on the physic-chemical expectations presented in Fig. 1.

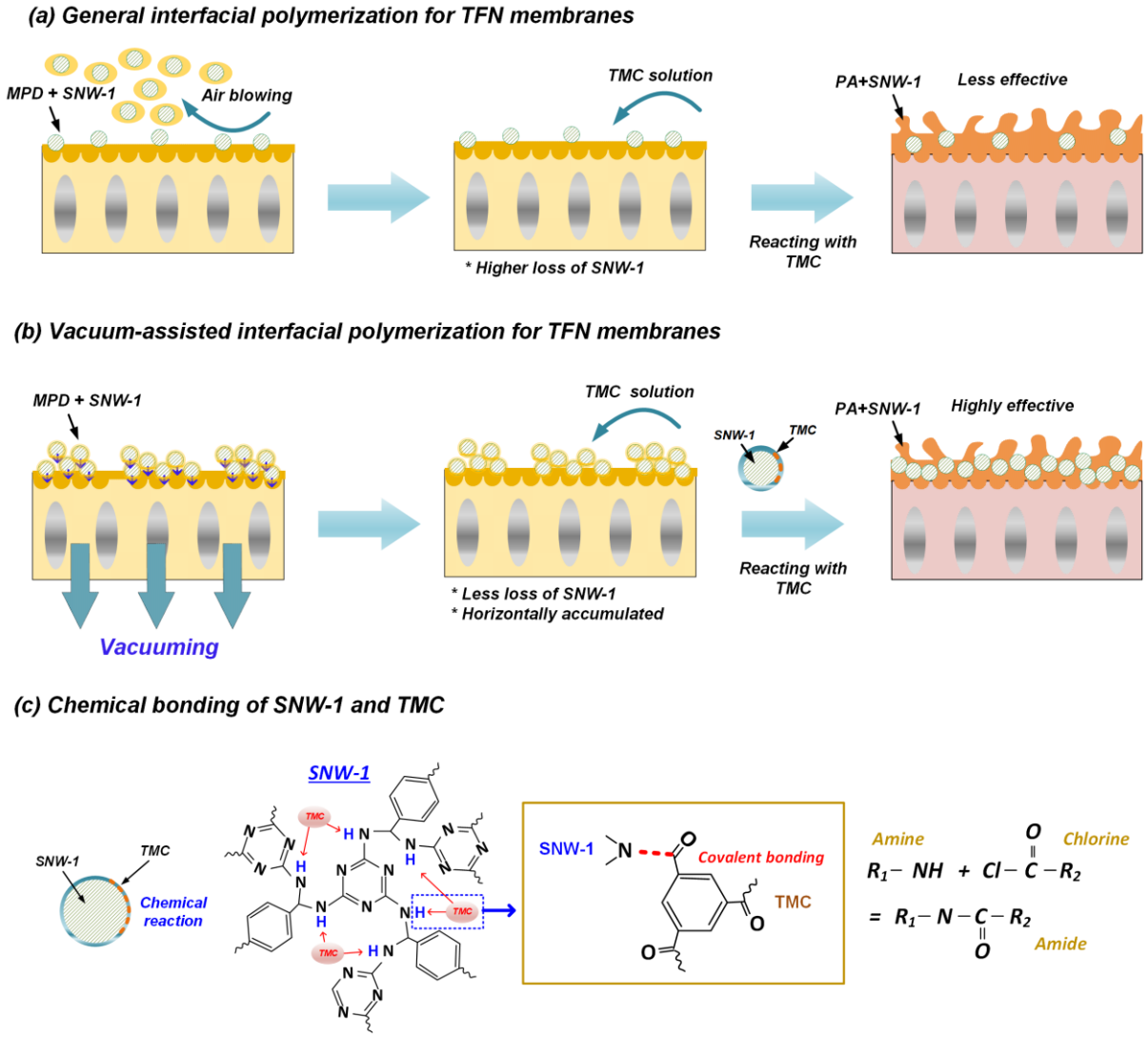

Figure 1 Comparison of expected phenomena about positioning SNW-1 inside PA layer under (a) general IP, and (b) the VAIP process, and expected chemical reaction with secondary amine groups in SNW-1 and acyl chloride groups in the TMC solution through the amide-based covalent bonding.

3.2 Characterizations of OSHF TFN membranes with SNW-1 NPs

Fig. 2 presents the surface images of the membrane substrates soaked with the MPD solution (denoted as $S0_s$) and MPD/SNW-1 (denoted as $S3_s$, $S5_s$, $S10_s$ and $S15_s$) blended solution after conducting the vacuum suction in the VAIP. $S0_s$ presented that there is no particulate on the surface of the MPD-soaked membrane substrate as expected. However, Fig. 3 shows that NPs clusters are visible across the surfaces of the MPD/SNW-1 soaked substrates. When the NPs' loadings are increased from $S3_s$ to $S15_s$, the number and size of the NPs clusters are proportionally increased due to NPs' aggregation. As shown in high magnified SEM images in Fig. 2, the NPs clusters were made of SNW-1 NPs in the size at around 40 nm which is similar with that presented in Fig. 2 (b). Although sub-50 nm SNW-1 particles were not distributed as a single-particle across the surface with the evidence of their aggregation, bunches of partially aggregated SNW-1 NPs were appropriately accumulated and distributed onto the surface prior to reacting with the TMC solution. However, $S15_s$ presented an aggregated NPs' dump at the size over 5 μm because of exceed loading of SNW-1 NPs, and this may subsequently deteriorate integrity of a PA layer. Although the SNW-1 bunches might be properly settled on the surface under the condition, the concentration of SNW-1 NPs may sensitively affect the quality of the PA composite layer. Therefore, it is necessary to optimize the dosing ratio of SNW-1 for fabricating suitable TFN membranes.

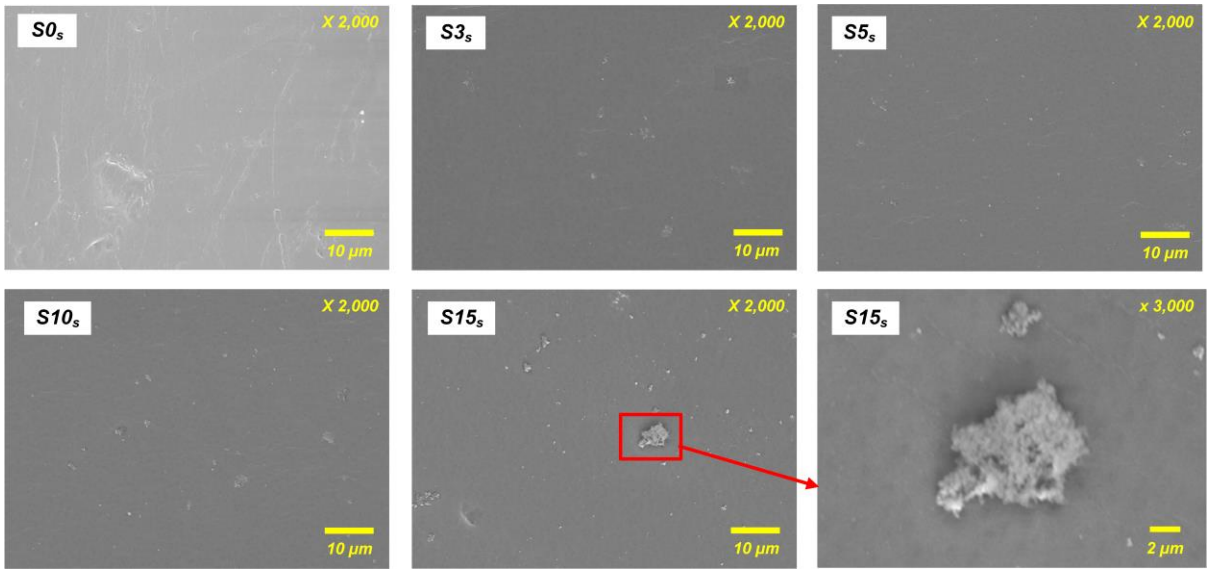

Figure 2 Surface images of MPD- ($S0_s$) and (b) MPD/SNW-1 ($S3_s$, $S5_s$, $S10_s$ and $S15_s$) soaked membrane substrates after conducting the vacuum suction in the VAIP process, and high-magnified image of aggregated SNW-1 NPs in $S15_s$.

Fig. 3 presents morphological images of the PA selective layers of all series of FO membranes. In these images, S0 membrane presented typical ridge-and-valley morphologies of the PA layer what many groups have reported [36, 54, 55]. With the addition of SNW-1 into a PA layer, S3 and S5 membranes demonstrate almost similar PA structures with that of neat TFC membrane (S0). The S10 and S15 membranes, on the other hand, showed bulged spots across the surface of the PA layers, but the other sides presented quite flat and smooth surface morphology. It means that the PA/SNW-1 composite layer might be aggregated by the higher SNW-1 NPs' loading in the VAIP, since SNW-1 NPs in MPD solution might interfere the chemical reaction with the MPD and TMC solution in IP process [56, 57]. Furthermore, the high-magnified SEM image of S15 in Fig. 3 (b) showed a lot of spherically bulged spots on the PA structure indicated by the yellow arrows compared to that of S0 (Fig. 3 (a)), which might be an evidence of the NPs incorporation or chemical interference. Therefore, it is

noteworthy to mention that excess NPs loading is able to cause deforming typical PA's ridge-and-valley structures, which may subsequently deteriorate membrane's selectivity.

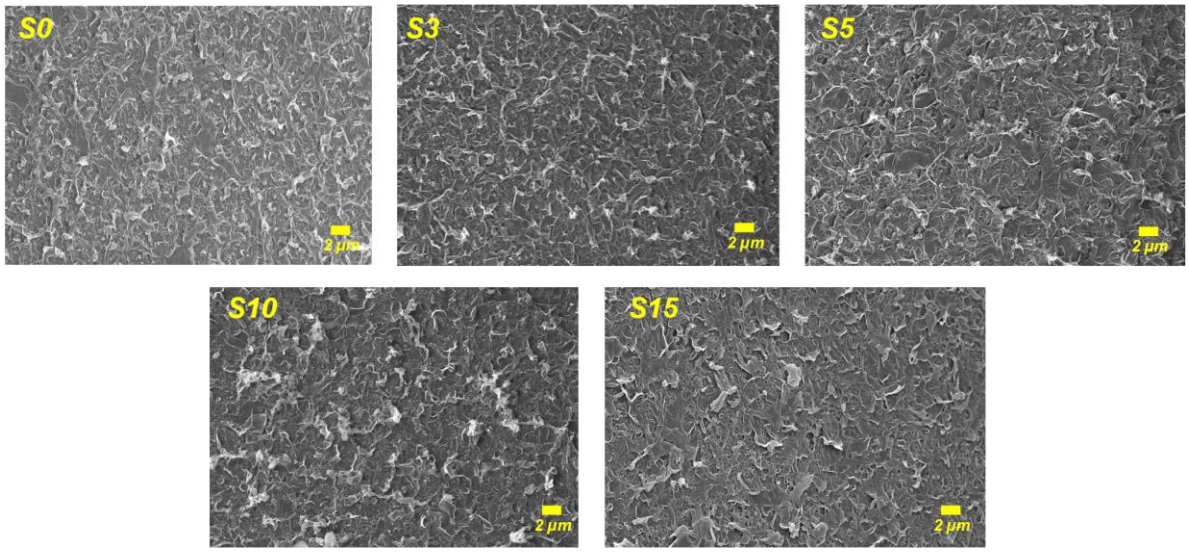

(a)

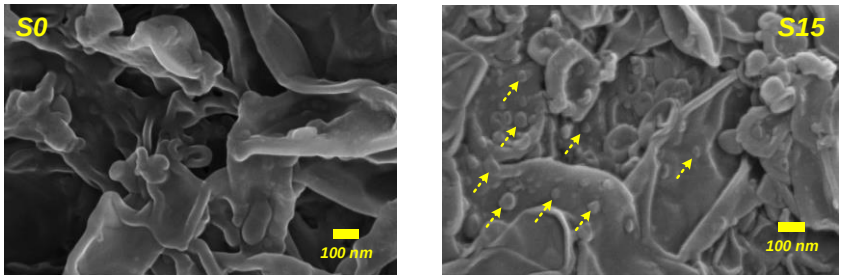

(b)

Figure 3 Morphological SEM images (x3,000) of the PA selective layer of TFC (S0) and TFN (S3, 5, 10, and 15) membrane samples (a), and high-magnification images (x50,000) of particle-free S0 (Left) and S15 with observing SNW-1 NPs (Right) inside the PA layer (b).

Using the AFM analysis, the 3D images and mean roughness (R_a) of the surfaces of selected OSHF TFN membranes (S0, S10 and S15) were produced as shown in Fig. 4(a). For particle-free S0 membrane, the ridge-valley-structure was shown in 3D image, and its R_a was

107.2 nm. In comparison of AFM results, it confirmed that the TFC membrane possesses the smoothest active surface, and R_a values of the TFN membranes were proportionally varied from 107.2 nm of S0 to 135.6 nm of S15 with an increase of SNW-1 loading. Higher roughness from the increase of SNW-1 loading may beneficially contribute to increasing membrane's surface area, however, it is required to optimize nanofiller's loading not to damage the thin PA layer by the incorporated fillers. Hydrophilicity of membrane's active layer was examined to investigate the water affinity of the PA composite layer incorporated with SNW-1 NPs. As shown in Fig. 4 (b), the contact angle values of SNW-1 incorporated membranes (S3, 5, 10 and 15) below 60° were lower than that of pristine one (S0) at 73.8°, since SNW-1 NPs possess hydrophilic amine-rich groups on their surface. However, with an increase of SNW-1 loading, the contact angles were slightly increased from 51° to 56°, although loading of the hydrophilic SNW-1 NPs was increased. As shown in Fig. 3 and Fig. 4 (a), the rough morphology on the surface of the SNW-1 composite PA layer might result from the protrusion of SNW-1 NPs, and it may cause to increase contact angle of water droplets because of trapped air pockets in rough valleys [37, 58]. Therefore, in the increase of SNW-1 loading into a PA layer, the composite PA layer would be altered to be rougher and hydrophilic due to its morphological structure and chemical functionality which may be beneficial for enhancing membrane's water permeability [46].

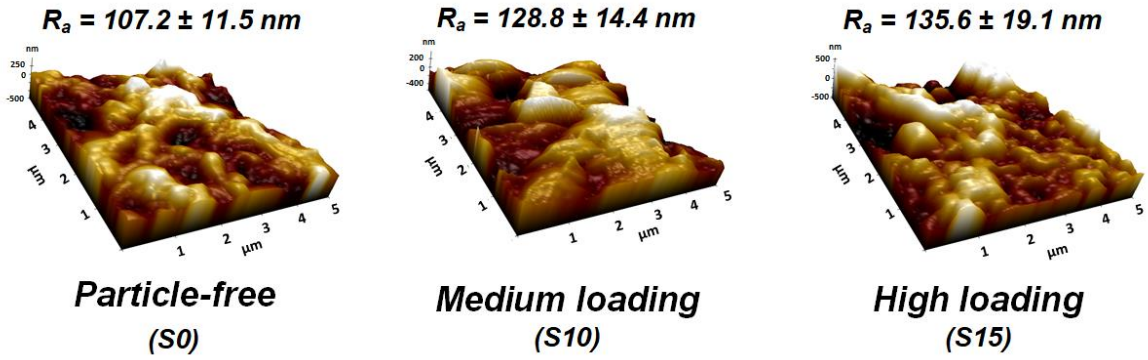

(a)

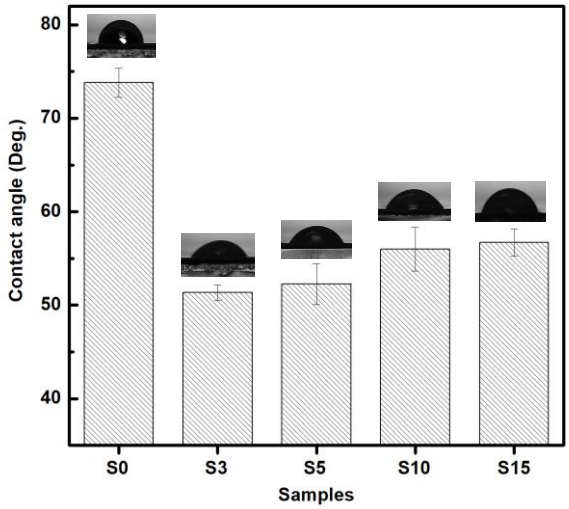

(b)

Figure 4 AFM images and average roughness of selected membrane samples according to SNW-1loading (a), and comparison of the contact angle of OSHF TFC and TFN membranes using SNW-1 nanoparticles (b).

The chemical analysis on the surface of the TFC and TFN membranes was conducted using FT-IR in order to investigate the existence of SNW-1 NPs and chemical changes of nanocomposite PA layer with SNW-1. Fig. 5 presents IR spectrums of TFC and TFN membranes incorporated with SNW-1 NPs. The IR spectrums of the TFC membrane clearly presented some representative peaks of a PES substrate at 1,150 cm^{-1} for C-SO_2-C stretch and at 1,240 cm^{-1} for C-O-C stretch and a thin PA layer between 1,505 and 1,540 cm^{-1} for amide II

(C-N stretch), 1610 cm^{-1} for the aromatic ring from the amide bonding and between 1,650 and 1,665 cm^{-1} for amide I [46]. Therefore, these peaks were considered to validate the PA layer of the OSHF TFC membranes. For TFN membranes with SNW-1, the intensity of the amide II's peak at 1540 cm^{-1} was proportionally increased when the SNW-1 loading was increased due to the increment of amide bonding from SNW-1. Furthermore, the specific peaks at 1,460 and 1,535 cm^{-1} were distinguished in the TFN membranes with higher loading of SNW-1, which is identified as triazine rings from SNW-1 [46]. In addition, the IR peaks at 1480 cm^{-1} presented in only TFN membranes represent C-N vibration of the semicircle stretching of the triazine ring from SNW-1. These IR results verify that the SNW-1 NPs were successfully incorporated into the thin PA layer.

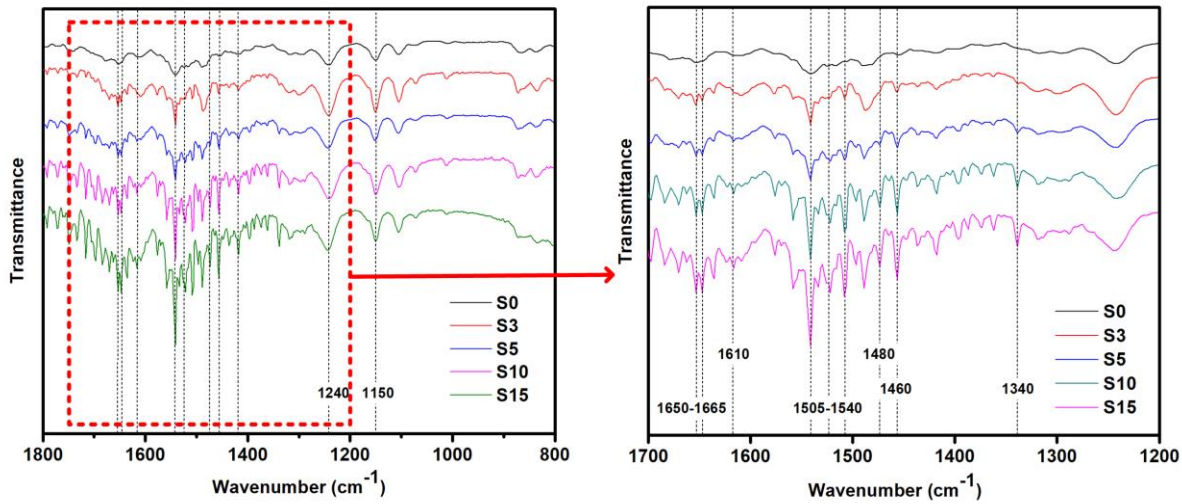

Figure 5 IR spectrums (Left: 800–1800 cm^{-1} and Right: 1200–1700 cm^{-1}) of OSHF TFC (S0) and TFN membranes using SNW-1 nanoparticles (S3, S5, S10 and S15).

3.3 FO performance of OSHF TFN membranes with SNW-1 NPs

The key FO performance of the TFC and TFN membranes were determined and evaluated under the FO operation (AL-FS orientation) using the lab-scale FO unit. The water flux and SRSF of series of the TFC (S0) and TFN (S3, 5, 10 and 15) membranes are shown in Fig. 6. The neat TFC membrane (S0) exhibited the water flux at 25.5 L m^{-2} h^{-1} and SRSF at 0.21 g L^{-1}. For TFN SNW-1 membranes, the water flux was gradually increased with no sacrifice of the SRSF, when the particle loading was increased up to 0.001 wt%. At 0.001 wt. %, S10 presented the highest water flux at 31.5 L m^{-2} h^{-1} (Improved 24% of the water flux of S0) with the relatively low SRSF at 0.18 g L^{-1} in series of TFN membranes. This result implies that the SNW-1 particles inside PA layer may contribute to modifying intrinsic transport property of the PA layer due to their unique characteristics such as porous frameworks themselves and hydrophilic nature, which are preferable for enhancing water transport. In addition, the SNW-1 might contribute to increase the free volume of the PA composite layer due to the incompatibility with a PA polymeric structure. However, increasing the SNW-1 loading beyond the optimal value at 0.001 wt.% deteriorated the FO performance of the OSHF TFN membranes. In particular, the water flux of S15 declined to 22.6 L m^{-2} h^{-1}, and its SRSF increased to 0.41 g L^{-1}. The overloading of SNW-1 NPs inside a PA layer formed a defective the PA layer, which reduced membrane selectivity. Consequently, the osmotic driving force across the membrane decreased, which resulted in lower water flux. Therefore, it can be established based on the FO performance that the optimal SNW-1 loading for preparing the OSHF TFN membrane is 0.001 wt.%."

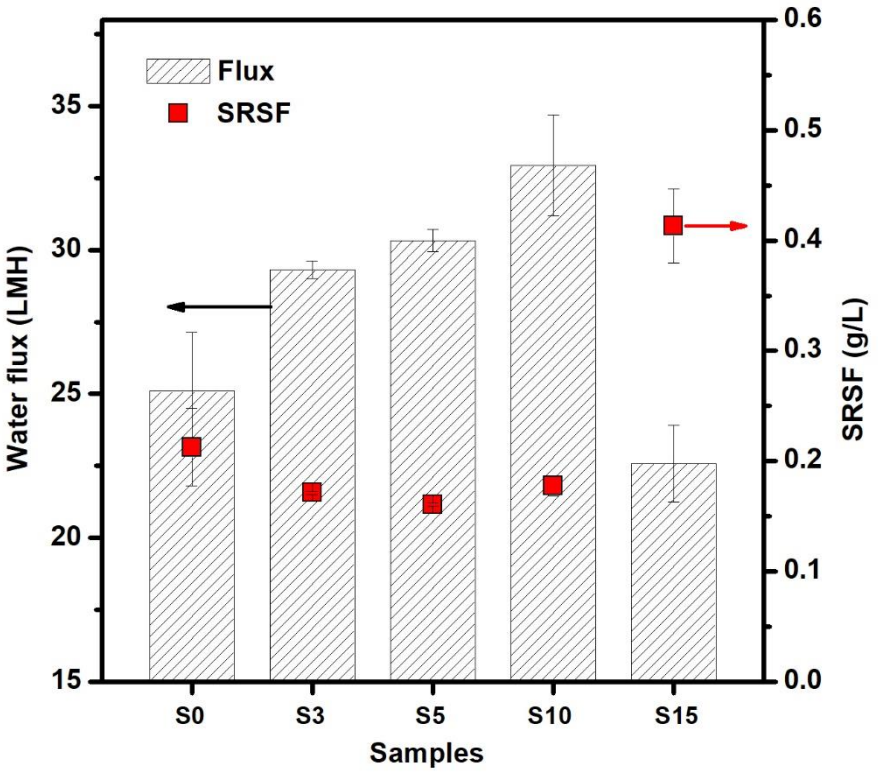

Figure 6 Comparison of key FO performances (water flux - Bar, and SRSF- Red dot) of OSHF TFC (S0) and TFN membranes according to different SNW-1 loading from 0 to 0.015 wt.%.

The comparative profiles of water flux and SRSF of the particle-free OSHF TFC (S0) and the best OSHF TFN membrane (S10) as a function of NaCl concentration from 0.5 to 2 M in a draw stream were determined in Fig. 7. The water fluxes of these membranes were proportionally increased due to a constant increase of the osmotic pressure as their driving force. However, the trends of SRSF results were stably maintained regardless of the difference of the driving force, as the trade-off relationship between water permeability and ion selectivity was retained even though the driving force was changed in FO operation. In the comparison, all water fluxes of S10 in all range of DS concentrations were higher than those of S0 due to higher water permeability of S10 as expected. As a result, S10 exhibited the highest water flux of 42.8 L m^{-2} h^{-1} with a stable SRSF at 0.22 g L^{-1} using 2 M NaCl solution as DS.

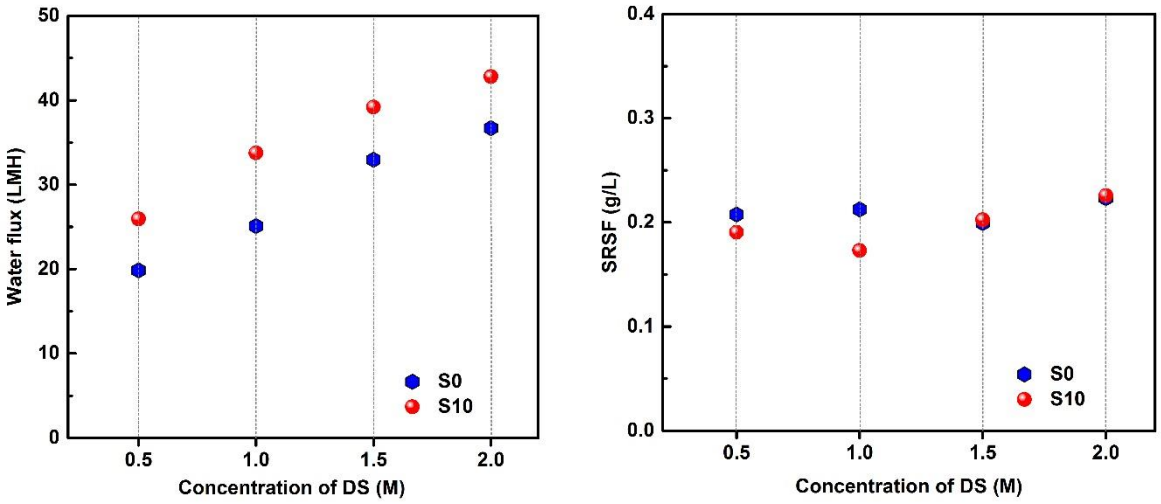

(a) (b)

Figure 7 (a) water flux and (b) SRSF profiles of S0 (TFC) and S10 (TFN) OSHF membranes according to different concentration of DS from 0.5 to 2 M.

Using the profiles in Fig.7, the intrinsic transport properties of the OSHF membranes (S0 and S10) were estimated by the FO model algorithm developed by Tiraferri and his colleagues [52]. Table 2 presents calculated water permeability (*A*), solute permeability coefficient (*B*), intrinsic selectivity (*B/A*) and structural parameter (S) of the OSHF TFC (S0) and the best OSHF TFN (S10) membranes. The *A* value of S10 at 2.37 L^{-1} m^{-2} h^{-1} bar^{-1} was higher than that of S0 at 1.68 L^{-1} m^{-2} h^{-1} bar^{-1}. However, the intrinsic selectivity of S10 at 0.18 bar was almost similar with that of S0 at 0.17 bar, which implies that the water permeability of S10 was improved with retaining ion selectivity compared to those of S0. The *S* value of S10 was similar with that of S0 due to the use of the same membrane substrates.

406 **Table 2** Intrinsic transport properties of selected OSHF TFN FO membranes (estimated by the
407 model calculation using the FO performance presented in Fig. 7)

FO membranes	*A* ($Lm^{-2}h^{-1}bar^{-1}$)	*B* ($Lm^{-2}h^{-1}$)	*B/A* (bar)	*S* (μm)
S0 (Pristine)	1.68	0.30	0.18	214
S10 (Best)	2.37	0.41	0.17	201

408

409 Most TFN membranes have been concerned about degrade of the PA selective layer over
410 the operation time due to delamination of NPs from the thin PA layer. The long-term
411 performance test of the best OSHF TFN membrane was thus conducted in order to further
412 investigate the membrane's stability under FO operation. For TFN membranes, it is necessary
413 to clearly show the FO performance in long-term operation for evaluating the membrane's
414 stability, due to the risk of releasing nanofillers from a PA composite layer under the crossflow
415 stream in FO operation, which may partially damage the PA active layer. Fig. 8 presents the
416 water flux of S10 in the long-term operation for 72 h. The S10 exhibited a remarkably stable
417 water flux for the period. This result shows that incorporated nanofillers (SNW-1) in S10 were
418 strongly linked with the PA matrix so that there is no concern about the deterioration of the FO
419 performance under a long-term operation. Therefore, the optimum membrane (S10) is able to
420 offer great potential for practical FO applications.

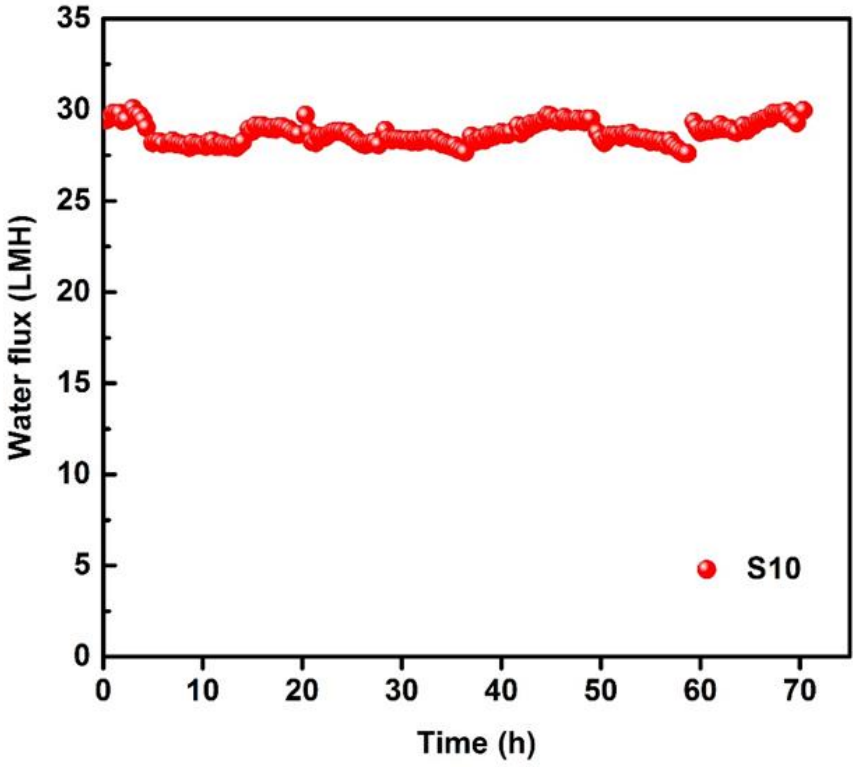

421

422 **Figure 8** Water flux of the best membrane candidate (S10) for 72 h in order to evaluate the
423 membrane's stability. The DS and FS was 1 M NaCl solution and DI water, respectively. These
424 solutions were refreshed every 4 h in the operation for 72 h in order to maintain the osmotic
425 driving force.

426

427

4 Conclusions

One COF material, SNW-1 was successfully applied to the development of novel OSHF TFN membranes for FO applications. In particular, the SNW-1 NPs were properly incorporated into the PA layer under the VAIP process with performance of the TFN membranes significantly improved with no detrimental issue of ion selectivity. The expected mechanisms for incorporating the SNW-1 NPs into PA layer in our hypothesis were successfully demonstrated based on the analysis and experimental results. The SNW-1 NPs were stacked and accumulated on the outer surface of HF substrates with minimum loss of particles by the vacuum pressure. Furthermore, the secondary amine groups in SNW-1 and acyl chloride groups in the TMC solution might chemically react to form an amide layer via the covalent bonding. These expected phenomena might strongly support to form a defect-free PA nanocomposite layer with SNW-1. The SNW-1 loading was manipulated and optimized in the extremely low range from 0 to 0.0015 wt.%, as such S10 sample (SNW-1 at 0.001 wt.%) exhibited the best FO performance with the highest water flux at 31.5 L m^{-2} h^{-1} and reasonable SRSF at 0.18 g L^{-1} in series of TFN membranes. The enhanced FO performance was attributed to the unique nature of SNW-1 itself like highly porous framework morphology and amine-based hydrophilic property, and good integrity of produced PA composite layer with no sacrifice of ion selectivity. The optimum TFN membrane (S10) exhibited high water flux at around 30 L m^{-2} h^{-1} and excellent stability of the FO performance with no decline of the water flux in the long-term operation for 72 h. Through the long-term experiment, it is noteworthy to mention that the optimum TFN membrane (S10) demonstrate the strong durability for its commercial application. These findings prove that the optimum sample (S10) can be a promising candidate to produce highly permeable FO performances for desalination and water treatment.

5 Acknowledgement

This research was supported by a grant from the Australia Research Council (ARC) Future Fellowship (FT140101208) and Discovery Early Career Researcher Award (DECRA, DE180100130). This work was supported by Korea Environment Industry & Technology Institute (KEITI) through Industrial Facilities & Infrastructure Research Program, funded by Korea Ministry of Environment (MOE) (1485016285).

6. References

[1] A. Achilli, J.L. Prante, N.T. Hancock, E.B. Maxwell, A.E. Childress, Experimental Results from RO-PRO: A Next Generation System for Low-Energy Desalination, Environmental Science & Technology, 48 (2014) 6437-6443.

[2] S. Phuntsho, H.K. Shon, T. Majeed, I. El Saliby, S. Vigneswaran, J. Kandasamy, S. Hong, S. Lee, Blended Fertilizers as Draw Solutions for Fertilizer-Drawn Forward Osmosis Desalination, Environmental Science & Technology, 46 (2012) 4567-4575.

[3] D.J. Johnson, W.A. Suwaileh, A.W. Mohammed, N. Hilal, Osmotic's potential: An overview of draw solutes for forward osmosis, Desalination, 434 (2018) 100-120.

[4] A.M. Awad, R. Jalab, J. Minier-Matar, S. Adham, M.S. Nasser, S.J. Judd, The status of forward osmosis technology implementation, Desalination, 461 (2019) 10-21.

[5] A.J. Ansari, F.I. Hai, W. Guo, H.H. Ngo, W.E. Price, L.D. Nghiem, Selection of forward osmosis draw solutes for subsequent integration with anaerobic treatment to facilitate resource recovery from wastewater, Bioresource Technology, 191 (2015) 30-36.

[6] W. Luo, H.V. Phan, G. Li, F.I. Hai, W.E. Price, M. Elimelech, L.D. Nghiem, An Osmotic Membrane Bioreactor–Membrane Distillation System for Simultaneous Wastewater Reuse and Seawater Desalination: Performance and Implications, Environmental Science & Technology, 51 (2017) 14311-14320.

[7] J. Seo, Y.M. Kim, S.H. Chae, S.J. Lim, H. Park, J.H. Kim, An optimization strategy for a forward osmosis-reverse osmosis hybrid process for wastewater reuse and seawater desalination: A modeling study, Desalination, 463 (2019) 40-49.

[8] V. Sant'Anna, L.D.F. Marczak, I.C. Tessaro, Membrane concentration of liquid foods by forward osmosis: Process and quality view, Journal of Food Engineering, 111 (2012) 483-489.

[9] S.L. Plata, A.E. Childress, Limiting power density in pressure-retarded osmosis: Observation and implications, Desalination, 467 (2019) 51-56.

[10] M.J. Park, S. Lim, R.R. Gonzales, S. Phuntsho, D.S. Han, A. Abdel-Wahab, S. Adham, H.K. Shon, Thin-film composite hollow fiber membranes incorporated with graphene oxide in polyethersulfone support layers for enhanced osmotic power density, Desalination, 464 (2019) 63-75.

[11] L. Chekli, S. Phuntsho, J.E. Kim, J. Kim, J.Y. Choi, J.-S. Choi, S. Kim, J.H. Kim, S. Hong, J. Sohn, H.K. Shon, A comprehensive review of hybrid forward osmosis systems: Performance, applications and future prospects, Journal of Membrane Science, 497 (2016) 430-449.

[12] W. Suwaileh, D. Johnson, N. Hilal, Brackish water desalination for agriculture: Assessing the performance of inorganic fertilizer draw solutions, Desalination, 456 (2019) 53-63.

[13] W. Suwaileh, D. Johnson, D. Jones, N. Hilal, An integrated fertilizer driven forward osmosis- renewables powered membrane distillation system for brackish water desalination: A combined experimental and theoretical approach, Desalination, 471 (2019) 114126.

[14] C.X. Guo, D. Zhao, Q. Zhao, P. Wang, X. Lu, Na+-functionalized carbon quantum dots: a new draw solute in forward osmosis for seawater desalination, Chemical Communications, 50 (2014) 7318-7321.

[15] Q. Ge, J. Su, G.L. Amy, T.-S. Chung, Exploration of polyelectrolytes as draw solutes in forward osmosis processes, Water Research, 46 (2012) 1318-1326.

[16] Q. Ge, M. Ling, T.-S. Chung, Draw solutions for forward osmosis processes: Developments, challenges, and prospects for the future, Journal of Membrane Science, 442 (2013) 225-237.

[17] M.S. Islam, S. Sultana, J.R. McCutcheon, M.S. Rahaman, Treatment of fracking wastewaters via forward osmosis: Evaluation of suitable organic draw solutions, Desalination, 452 (2019) 149-158.

512 [18] X. Liu, S. Qi, Y. Li, L. Yang, B. Cao, C.Y. Tang, Synthesis and characterization of novel
513 antibacterial silver nanocomposite nanofiltration and forward osmosis membranes based on
514 layer-by-layer assembly, Water Research, 47 (2013) 3081-3092.
515 [19] N. Akther, A. Sodiq, A. Giwa, S. Daer, H.A. Arafat, S.W. Hasan, Recent advancements
516 in forward osmosis desalination: A review, Chemical Engineering Journal, 281 (2015) 502-
517 522.
518 [20] J. Yin, B. Deng, Polymer-matrix nanocomposite membranes for water treatment, Journal
519 of Membrane Science, 479 (2015) 256-275.
520 [21] X. Liu, H.Y. Ng, Fabrication of layered silica–polysulfone mixed matrix substrate
521 membrane for enhancing performance of thin-film composite forward osmosis membrane,
522 Journal of Membrane Science, 481 (2015) 148-163.
523 [22] P. Xiao, L.D. Nghiem, Y. Yin, X.-M. Li, M. Zhang, G. Chen, J. Song, T. He, A sacrificial-
524 layer approach to fabricate polysulfone support for forward osmosis thin-film composite
525 membranes with reduced internal concentration polarisation, Journal of Membrane Science,
526 481 (2015) 106-114.
527 [23] D. Ma, S.B. Peh, G. Han, S.B. Chen, Thin-Film Nanocomposite (TFN) Membranes
528 Incorporated with Super-Hydrophilic Metal–Organic Framework (MOF) UiO-66: Toward
529 Enhancement of Water Flux and Salt Rejection, ACS Applied Materials & Interfaces, 9 (2017)
530 7523-7534.
531 [24] W. Sun, J. Shi, C. Chen, N. Li, Z. Xu, J. Li, H. Lv, X. Qian, L. Zhao, A review on organic–
532 inorganic hybrid nanocomposite membranes: a versatile tool to overcome the barriers of
533 forward osmosis, RSC Advances, 8 (2018) 10040-10056.
534 [25] H.B. Park, J. Kamcev, L.M. Robeson, M. Elimelech, B.D. Freeman, Maximizing the right
535 stuff: The trade-off between membrane permeability and selectivity, Science, 356 (2017).

[26] J. Duan, Y. Pan, F. Pacheco, E. Litwiller, Z. Lai, I. Pinnau, High-performance polyamide thin-film-nanocomposite reverse osmosis membranes containing hydrophobic zeolitic imidazolate framework-8, Journal of Membrane Science, 476 (2015) 303-310.

[27] J. Yin, G. Zhu, B. Deng, Graphene oxide (GO) enhanced polyamide (PA) thin-film nanocomposite (TFN) membrane for water purification, Desalination, 379 (2016) 93-101.

[28] C. Zhang, K. Wei, W. Zhang, Y. Bai, Y. Sun, J. Gu, Graphene Oxide Quantum Dots Incorporated into a Thin Film Nanocomposite Membrane with High Flux and Antifouling Properties for Low-Pressure Nanofiltration, ACS Applied Materials & Interfaces, 9 (2017) 11082-11094.

[29] S.F. Anis, R. Hashaikeh, N. Hilal, Functional materials in desalination: A review, Desalination, 468 (2019) 114077.

[30] D. Li, Y. Yan, H. Wang, Recent advances in polymer and polymer composite membranes for reverse and forward osmosis processes, Progress in Polymer Science, 61 (2016) 104-155.

[31] A. Zirehpour, A. Rahimpour, M. Ulbricht, Nano-sized metal organic framework to improve the structural properties and desalination performance of thin film composite forward osmosis membrane, Journal of Membrane Science, 531 (2017) 59-67.

[32] M. Tian, Y.-N. Wang, R. Wang, A.G. Fane, Synthesis and characterization of thin film nanocomposite forward osmosis membranes supported by silica nanoparticle incorporated nanofibrous substrate, Desalination, 401 (2017) 142-150.

[33] N. Akther, S. Phuntsho, Y. Chen, N. Ghaffour, H.K. Shon, Recent advances in nanomaterial-modified polyamide thin-film composite membranes for forward osmosis processes, Journal of Membrane Science, 584 (2019) 20-45.

[34] H.-R. Chae, J. Lee, C.-H. Lee, I.-C. Kim, P.-K. Park, Graphene oxide-embedded thin-film composite reverse osmosis membrane with high flux, anti-biofouling, and chlorine resistance, Journal of Membrane Science, 483 (2015) 128-135.

[35] J. Balapanuru, K.K. Manga, W. Fu, I. Abdelwahab, G. Zhou, M. Li, H. Lu, K.P. Loh, Desalination properties of a free-standing, partially oxidized few-layer graphene membrane, Desalination, 451 (2019) 72-80.

[36] S. Lim, M.J. Park, S. Phuntsho, L.D. Tijing, G.M. Nisola, W.-G. Shim, W.-J. Chung, H.K. Shon, Dual-layered nanocomposite substrate membrane based on polysulfone/graphene oxide for mitigating internal concentration polarization in forward osmosis, Polymer, 110 (2017) 36-48.

[37] S. Lim, M.J. Park, S. Phuntsho, A. Mai-Prochnow, A.B. Murphy, D. Seo, H. Shon, Dual-layered nanocomposite membrane incorporating graphene oxide and halloysite nanotube for high osmotic power density and fouling resistance, Journal of Membrane Science, 564 (2018) 382-393.

[38] M. Amini, M. Jahanshahi, A. Rahimpour, Synthesis of novel thin film nanocomposite (TFN) forward osmosis membranes using functionalized multi-walled carbon nanotubes, Journal of Membrane Science, 435 (2013) 233-241.

[39] L. Dumée, J. Lee, K. Sears, B. Tardy, M. Duke, S. Gray, Fabrication of thin film composite poly(amide)-carbon-nanotube supported membranes for enhanced performance in osmotically driven desalination systems, Journal of Membrane Science, 427 (2013) 422-430.

[40] H. Sun, P. Wu, Tuning the functional groups of carbon quantum dots in thin film nanocomposite membranes for nanofiltration, Journal of Membrane Science, 564 (2018) 394-403.

[41] Y. Li, S. Li, K. Zhang, Influence of hydrophilic carbon dots on polyamide thin film nanocomposite reverse osmosis membranes, Journal of Membrane Science, 537 (2017) 42-53.

[42] T. Ormanci-Acar, F. Celebi, B. Keskin, O. Mutlu-Salmanlı, M. Agtas, T. Turken, A. Tufani, D.Y. Imer, G.O. Ince, T.U. Demir, Y.Z. Menceloglu, S. Unal, I. Koyuncu, Fabrication

585 and characterization of temperature and pH resistant thin film nanocomposite membranes
586 embedded with halloysite nanotubes for dye rejection, Desalination, 429 (2018) 20-32.
587 [43] M. Rezaei-DashtArzhandi, M.H. Sarrafzadeh, P.S. Goh, W.J. Lau, A.F. Ismail, M.A.
588 Mohamed, Development of novel thin film nanocomposite forward osmosis membranes
589 containing halloysite/graphitic carbon nitride nanoparticles towards enhanced desalination
590 performance, Desalination, 447 (2018) 18-28.
591 [44] C. Wang, Z. Li, J. Chen, Z. Li, Y. Yin, L. Cao, Y. Zhong, H. Wu, Covalent organic
592 framework modified polyamide nanofiltration membrane with enhanced performance for
593 desalination, Journal of Membrane Science, 523 (2017) 273-281.
594 [45] L.F. Dumée, J.W. Maina, A. Merenda, R. Reis, L. He, L. Kong, Hybrid thin film nano-
595 composite membrane reactors for simultaneous separation and degradation of pesticides,
596 Journal of Membrane Science, 528 (2017) 217-224.
597 [46] N. Akther, S. Lim, V.H. Tran, S. Phuntsho, Y. Yang, T.-H. Bae, N. Ghaffour, H.K. Shon,
598 The effect of Schiff base network on the separation performance of thin film nanocomposite
599 forward osmosis membranes, Separation and Purification Technology, 217 (2019) 284-293.
600 [47] V.H. Tran, S. Lim, D.S. Han, N. Pathak, N. Akther, S. Phuntsho, H. Park, H.K. Shon,
601 Efficient fouling control using outer-selective hollow fiber thin-film composite membranes for
602 osmotic membrane bioreactor applications, Bioresource Technology, 282 (2019) 9-17.
603 [48] S. Lim, V.H. Tran, N. Akther, S. Phuntsho, H.K. Shon, Defect-free outer-selective hollow
604 fiber thin-film composite membranes for forward osmosis applications, Journal of Membrane
605 Science, 586 (2019) 281-291.
606 [49] V. Huy Tran, S. Lim, M. Jun Park, D. Suk Han, S. Phuntsho, H. Park, H. Matsuyama, H.
607 Kyong Shon, Fouling and performance of outer selective hollow fiber membrane in osmotic
608 membrane bioreactor: Cross flow and air scouring effects, Bioresource Technology, 295
609 (2020) 122303.

610 [50] M.G. Schwab, B. Fassbender, H.W. Spiess, A. Thomas, X. Feng, K. Müllen, Catalyst-free
611 preparation of melamine-based microporous polymer networks through Schiff base chemistry,
612 Journal of the American Chemical Society, 131 (2009) 7216-7217.
613 [51] S. Lim, V.H. Tran, N. Akther, S. Phuntsho, H.K. Shon, Defect-free outer-selective hollow
614 fiber thin-film composite membranes for forward osmosis applications, Journal of Membrane
615 Science, 586 (2019) 286-291.
616 [52] A. Tiraferri, N.Y. Yip, A.P. Straub, S. Romero-Vargas Castrillon, M. Elimelech, A
617 method for the simultaneous determination of transport and structural parameters of forward
618 osmosis membranes, Journal of Membrane Science, 444 (2013) 523-538.
619 [53] X. Gao, X. Zou, H. Ma, S. Meng, G. Zhu, Highly Selective and Permeable Porous Organic
620 Framework Membrane for CO2 Capture, Advanced Materials, 26 (2014) 3644-3648.
621 [54] H. Guo, Z. Yao, J. Wang, Z. Yang, X. Ma, C.Y. Tang, Polydopamine coating on a thin
622 film composite forward osmosis membrane for enhanced mass transport and antifouling
623 performance, Journal of Membrane Science, 551 (2018) 234-242.
624 [55] G. Han, Z.L. Cheng, T.-S. Chung, Thin-film composite (TFC) hollow fiber membrane
625 with double-polyamide active layers for internal concentration polarization and fouling
626 mitigation in osmotic processes, Journal of Membrane Science, 523 (2017) 497-504.
627 [56] M.I. Baig, P.G. Ingole, J.-d. Jeon, S.U. Hong, W.K. Choi, B. Jang, H.K. Lee, Water vapor
628 selective thin film nanocomposite membranes prepared by functionalized Silicon
629 nanoparticles, Desalination, 451 (2019) 59-71.
630 [57] M.R. De Guzman, M.B.M.Y. Ang, C.-L. Lai, C.A. Trilles, J.M. Pereira, R.R. Aquino, S.-
631 H. Huang, K.-R. Lee, Choice of Apposite Dispersing Medium for Silica Nanoparticles Leading
632 to Their Effective Embedment in Nanocomposite Nanofiltration Membranes, Industrial &
633 Engineering Chemistry Research, 58 (2019) 17937-17944.

[58] L.D. Tijing, Y.C. Woo, W.-G. Shim, T. He, J.-S. Choi, S.-H. Kim, H.K. Shon, Superhydrophobic nanofiber membrane containing carbon nanotubes for high-performance direct contact membrane distillation, Journal of Membrane Science, 502 (2016) 158-170.